$[C_5H_5MoS_2CN(CH_3)_2]_2(PF_6)_2$. The fluorosulfonate salt was slurried in MeOH, and NH_4PF_6 was added. The slurry was stirred for 1 h in an open beaker, and the solid was filtered off. This was carried out twice. The final solid was recrystallized from acetonitrile/methanol in the presence of NH_4PF_6, yield 80%. IR: 1585 (s, ν_{C-N}), 845, 560 cm^{-1} (PF_6). $\Lambda_M(CH_3CN)$ = 288 $cm^2/\Omega \cdot mol$. ^{13}C NMR (CD_3CN): δ 97.32 (CH_3), 118.31 (C_5H_5), S_2CN- not observed. Anal. Calcd for $C_{16}H_{22}N_2S_4Mo_2P_2F_{12}$: C, 22.54; H, 2.60; S, 15.04. Found: C, 22.57; H, 2.58; S, 15.12.

$[C_5H_5MoS_2CN(H)R]_2(X)_2$ (X = SO_3CF_3 or PF_6). The neutral dithiocarbonimidate complex (R = CH_3, C_4H_9) was dissolved in THF, and trifluoromethanesulfonic acid (~2.5 equiv) was added. After stirring for 2.5 h, the yellow-brown precipitate was filtered. R = CH_3: yield 85%. R = C_4H_9: yield 70%; IR 1565 cm^{-1} (s, ν_{C-N}); $\Lambda_M(CH_3CN)$ = 247 $cm^2/\Omega \cdot mol$. Each derivative was dissolved in MeOH, and the addition of excess NH_4PF_6 resulted in the precipitation of the bronze-colored PF_6^- salt. For R = CH_3: IR 3300 (m, ν_{N-H}), 2463 (w, ν_{H-H}), 1595 (s, ν_{C-N}), 845, 560 cm^{-1} (s, PF_6^-); $\Lambda_M(CH_3CN)$ = 284 $cm^2/\Omega \cdot mol$. Anal. Calcd for $C_{14}H_{18}N_2S_4Mo_2P_2F_{12}$: C, 20.40; H, 2.20; S, 15.56. Found: C, 20.62; H, 2.35; S, 15.51.

Reactions of $[C_5H_5MoS_2CNCH_3]_2$ with Ethene or Propene. $[C_5H_5MoS_2CNCH_3]_2$ (0.25 g, 0.47 mmol) was dissolved in 25 mL of $CHCl_3$, and ~2 atm of the appropriate gas was added to a 100-mL reaction tube equipped with a vacuum valve. The solution was stirred for 8 days at 25 °C. The solution was then filtered, the filtrate was reduced in volume, and the resulting solid was analyzed by NMR. For the ethene case, ~74% of the product was $[C_5H_5MoSC_2H_4S]_2$; ~26% of a mixed-bridge derivative $(C_5H_5)_2Mo_2(S_2CNCH_3)(SC_2H_4S)$ was present. Yields of the dithiolate bridged species may be increased by exhausting the atmosphere of the reaction tube and recharging with the appropriate gas.

Determination of Equilibrium Constants. Samples of $[C_5H_4CH_3MoSC_2H_4S]_2$ (0.025 g) were dissolved in 0.70 mL of $CDCl_3$ in three NMR tubes, and 1, 2, and 3 equiv of $C_6H_5CH_2NC$ were added, respectively. The solutions were degassed in three freeze–pump–thaw cycles and the tubes were flame sealed. The systems were allowed to reach equilibrium for 10–14 days at 25 °C and for 6–24 h in the probe. NMR spectra were obtained at 35 °C. Averages of integration values were determined from several scans of each sample.

Reactions with Reducing Agents. A. $[C_5H_5MoS_2CNR]_2$ (R = CH_3 or $C_6H_5CH_2$) was dissolved in $CHCl_3$ and 1–2 atm of H_2 was added. The solution was stirred at 60–80 °C for 24 h. The dark brown products of low solubility which were formed were not characterized. No amines were detected by NMR or GC.

B. The above reaction was repeated with the addition of excess RNC. Similar results were observed.

C. $[C_5H_5MoS_2CNR]_2$ was dissolved in $CDCl_3$ in a bomb reactor and 800–900 psi H_2 was added. The solution was stirred for 36 h at 25 °C. Largely insoluble products were formed; no amines were detected by NMR.

D. The reaction in C was repeated with the addition of excess RNC. No decomposition occurred in this case; no amines were detected by NMR.

E. $[C_5H_5MoS_2CNCH_2C_6H_5]_2$ (0.06 mmol) was slurried in THF under a nitrogen atmosphere and $NaBH_4$ (0.6 mmol) was added. The solution was refluxed for 36 h. Most of the dithiocarbonimidate complex was recovered; no amines were detected by NMR.

Attempted Reactions with CO. A. $[C_5H_5MoS_2CNCH_2C_6H_5]_2$ was dissolved in $CDCl_3$ and 1–2 atm CO was added. The solution was stirred at 70 °C for 48 h. The NMR spectrum of the solution indicated that no free isocyanide was present and the spectrum of the starting complex was unchanged. Similar results were observed with 800 psi CO at 25 °C and after purging a solution with CO for 48 h.

B. The reaction in A was repeated in a bomb reactor with 900 psi CO/H_2 (1:3 molar ratio). The solution was stirred for 48 h at 25 °C. No pressure change occurred and no hydrogenated products were detected by GC. Dark, insoluble molybdenum-containing products were not characterized.

Acknowledgments. Support for this work from the donors of the Petroleum Research Fund, administered by the American Chemical Society, from the National Institutes of Health (Grant GM-25122), and from the Department of Energy, Fossil Energy Division, is gratefully acknowledged. We thank Martin Ashley for obtaining the ^{13}C NMR spectra.

Low-Temperature Crystal and Molecular Structure of Tetracarbonyl[2-bromoheptahydrotriborato(1-)]manganese, $(CO)_4MnB_3H_7Br$, and a ^1H NMR Study of the Kinetics of Its Intramolecular Hydrogen Exchange in Solution

Michael W. Chen, Joseph C. Calabrese, Donald F. Gaines,* and David F. Hillenbrand

Contribution from the Department of Chemistry, University of Wisconsin—Madison, Madison, Wisconsin 53706. *Received January 2, 1980*

Abstract: The −100 °C X-ray-determined structure of $(CO)_4MnB_3H_7Br$ shows the bidentate B_3H_7Br ligand (in which the Br atom is attached to the unique B atom in an exo position) bound by two Mn–H–B bridge bonds to the octahedrally coordinated manganese in molecules of C_s molecular symmetry. The orthorhombic crystals, of space group *Pmcn*, have unit cell parameters a = 7.658 (3) Å, b = 9.084 (3) Å, c = 15.426 (5) Å, V = 1073 (1) Å^3, and Z = 4. The X-ray structure was solved by heavy-atom methods and refined to R_1 = 0.0536 and R_2 = 0.0652 for 1473 independent θ–2θ observed reflections. The boron-bound hydrogen atoms in $(CO)_4MnB_3H_7Br$ undergo internal exchange in solution at rates amenable to study by NMR. Kinetic activation parameters for the intramolecular hydrogen-exchange process in $(CO)_4MnB_3H_7Br$, based on an analysis of $^1H\{^{11}B\}$ variable-temperature NMR spectra, are $\Delta G^{\ddagger}$(23 °C) = 12.2 ± 0.1 kcal/mol, $\Delta H^{\ddagger}$ = 10.7 ± 0.7 kcal/mol, and $\Delta S^{\ddagger}$ = −5.1 ± 2.7 eu. Mechanistic proposals for the intramolecular hydrogen-exchange processes in $(CO)_4MnB_3H_7Br$ and the related molecules $(CO)_3MnB_3H_8$ and $(CO)_4MnB_3H_8$ are discussed.

Introduction

Tetracarbonyl[bromoheptahydrotriborato(1-)]manganese, $(CO)_4MnB_3H_7Br$, is a moderately air-stable, light yellow solid (mp 48–49 °C, dec) which can be prepared by direct halogenation of tetracarbonyl[octahydrotriborato(1-)]manganese, $(CO)_4MnB_3H_8$.[1] The room-temperature ^{11}B NMR spectrum of $(CO)_4MnB_3H_7Br$ indicates that the B_3H_7Br ligand is bidentate and is halogenated at the unique boron atom B(2). In addition, a rapid intramolecular hydrogen exchange among the boron-bound hydrogens is indicated by the ^1H NMR spectrum, while the hy-

(1) Gaines, D. F.; Hildebrandt, S. J. *Inorg. Chem.* **1978**, *17*, 794–806.

0002-7863/80/1502-4928$01.00/0

Table I. Crystallographic Data for $Mn(CO)_4B_3H_7Br$ at −100 °C

crystn method	sublimation at ambient temperature, 10^{-4} torr
cryst shape/color	cubic/light yellow
mol wt	286.3
data collectn temp, °C	−100 ± 2
radiatn (graphite monochromator)	Mo Kα
scan speed, deg/min	2 to 24
bkgd to scan time ratio	2:3
range of 2θ, deg	3–55
total reflctns	1649
independent reflctns	1473
independent obsd reflctns	892
cryst system	orthorhombic
systematic absences	$hk0$, $h + k$ odd; $h0l$, l odd ($h00$, h odd; $0k0$, k odd; $00l$, l odd)
space group	*Pmcn* (nonstandard setting[5] *Pnma*, No. 62)
equiv positns	x, y, z; $^1/_2 - x, y, z$; $x, ^1/_2 - y, ^1/_2 + z$; $^1/_2 + x, ^1/_2 + y, ^1/_2 - z$; $^1/_2 - x, ^1/_2 - y, ^1/_2 + z$; $-x, ^1/_2 + y, ^1/_2 - z$; $^1/_2 - x, -y, -z$; $-x, -y, -z$
special positn, *m*	0, 0, 0; $^1/_2$, 0, 0; 0, $^1/_2$, $^1/_2$; $^1/_2$, $^1/_2$, $^1/_2$
no. of molecules/unit cell	4
calcd density (−100 °C)	1.771 g/cm^3
lattice const (errors)	
a, Å	7.658 (3)
b, Å	9.084 (3)
c, Å	15.426 (5)
V, Å^3	1073 (1)
data to parameter ratio	11.99
final discrepancy values	
R_1	0.0536
R_2	0.0652

drogens involved in the Mn–H–B bridge bonds appear as static metal hydride like hydrogens. At temperatures below −20 °C, the ^{11}B and ^1H NMR spectra show the presence of a single static isomer, but they do not allow assignment of an endo- or exo-halogen position on the unique boron atom, B(2).

Several investigations were undertaken in order to examine the internal hydrogen exchange occurring in $(CO)_4MnB_3H_7Br$ and to compare it in detail with hydrogen exchange in other manganese octahydrotriborate complexes such as $(CO)_4MnB_3H_8$, $(CO)_3MnB_3H_8$, and $(CO)_4MnB_3H_7Cl$. First, a low-temperature single-crystal X-ray structural study of $(CO)_4MnB_3H_7Br$ was undertaken. Second, the variable-temperature ^1H NMR spectra of $(CO)_4MnB_3H_7Br$ were reinvestigated under conditions of essentially complete ^{11}B decoupling. These NMR spectra were then subjected to a line-shape analysis to determine activation parameters as an aid to the elucidation of the intramolecular hydrogen-exchange mechanisms in this and related octahydrotriborate complexes.

Experimental Section

Single crystals of $(CO)_4MnB_3H_7Br$[1] were grown as large yellow blocks by slow sublimation at 21 °C and 10^{-3}-torr pressure to a water cooled probe at 11 °C. Selected crystals were mounted in thin-walled Lindemann soft-glass capillaries under argon. A suitable crystal was then aligned on a NOVA computer-controlled Syntex P$\bar{1}$ four-circle diffractometer equipped with a Syntex LT-1 low-temperature accessory. A data set was successfully acquired at a regulated temperature of −100 °C (±2 °C). With use of standard Syntex software routines,[2] the crystal was

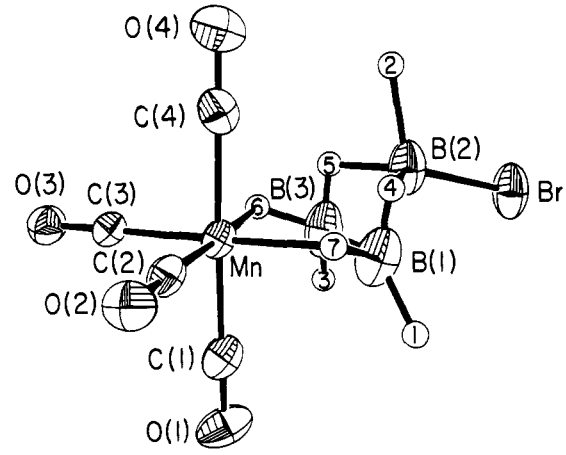

Figure 1. The static molecular structure of $(CO)_4MnB_3H_7Br$ showing the atom-numbering system used in this study. In this ORTEP representation, the atomic thermal ellipsoids are plotted at the 40% probability contour. The hydrogen atoms are shown as hard spheres of 0.15-Å radius.

centered and then indexed in *h*, *k*, and *l*, from which lattice parameters were determined. A summary of experimental conditions and final results of the data collection are presented in Table I.

NMR samples of $(CO)_4MnB_3H_7Br$, $(CO)_4MnB_3H_8$, and $(CO)_3MnB_3H_8$ (5-mm o.d.) were prepared by using standard Schlenk and high-vacuum procedures. The toluene-d_8 solvent was degassed and distilled in vacuo from $LiAlH_4$ directly into the sample tubes. The NMR samples were sealed under vacuum at −196 °C and stored at −78 °C until use.

Variable-temperature ^{11}B spin-decoupled 270-MHz ^1H NMR spectra were obtained by using a Bruker WH-270 high-resolution NMR spectrometer equipped with a BNC-12 computer. Temperatures were maintained to within ±0.2 °C by a Bruker B-ST 100/700 variable-temperature controller and were checked with an external thermocouple at the start and finish of each experimental observation. ^{11}B spin decoupling was accomplished by using a Bruker B-BM-1 broad-band modulator, a Bruker B-FS 100 frequency synthesizer, and a Bruker B-LV 80 selective power amplifier. The standard Bruker heteronuclear decoupling package was combined with a double-balanced mixer[3] driven by a Hewlett-Packard HP 3301A function generator in order to decouple both ^{11}B positions while collecting ^1H data.

Solution and Refinement of the Structure

The solution of the structure was accomplished by using standard Fourier and heavy-atom techniques.[4] All manipulation and reduction was accomplished by using an absorption-corrected data set. Using coordinates for the Br and Mn atoms provided by an ambient-temperature data set, a single Fourier synthesis revealed the positions of all nonhydrogen atoms. Following several cycles of full-matrix least-squares refinement, in which positional and isotropic thermal parameters for the nonhydrogen atoms were varied, a difference map gave postitions for the BHB bridge hydrogens and the hydrogen attached to the unique boron. Additional least-squares refinement, in which the nonhydrogen atoms were allowed to vary in both positional and anisotropic thermal parameters, led to a difference map in which all the hydrogen atoms could be located. Final discrepancy values converged at $R_1 = 0.0536$[6] and $R_2 = 0.0652$.[7] A final difference map indicated a peak of 1.125 electrons below the exo-halogen position and a peak of 0.985 electrons at a site centered immediately below the B_3 triangle. The final data to parameter ratio was 12:1. Scattering factors used for all atoms are those of Hanson et al.[8] All least-squares refinement was based on the minimization of $\sum w_2(|F_o| - |F_c|)^2$, with weights w_i equal to $1/\sigma(F_o)^2$. Estimated standard deviations in bond lengths, angles, and thermal parameters are calculated

(2) Sparks, R. A. "P$\bar{1}$ Autodiffractometer Operations Manual"; Syntex Analytical Instruments Division: Cupertino, CA, 1970.

(3) Designed and constructed by M. V. Kontney, Department of Chemistry, University of Wisconsin–Madison.

(4) Programs used in the structural determination and refinements included MAP, MIRAGE, and REFINE, written by J. C. Calabrese, and ORTEP II, the C. K. Johnson thermal ellipsoid plotting program.

(5) Henry, N. F. M., Lonsdale, K., Eds. "International Tables for X-Ray Crystallography"; Kynoch Press: Birmingham, England, 1952; Vol. 1.

(6) $R_1 = \sum(|F_o| - |F_c|)/|F_o|$.

(7) $R_2 = [\sum w_i(|F_o| - |F_c|)^2/\sum|F_o|^2]^{1/2}$, where weights $w_i = 1/\sigma(F_o)^2$.

(8) Hanson, H. P.; Herman, F.; Lea, J. D.; Skillman, S. *Acta Crystallogr.* **1964**, *17*, 1040–44.

Table II. Final Atomic Positional Parameters ($\times 10^4$) and Isotropic Thermal Parameters[a] ($Å^2$) for $(CO)_4MnB_3H_7Br$

atom	x	y	z	atom	x	y	z
Br	2500	1043 (1)	3383 (1)	C(2)	−783 (8)	−2975 (6)	−13 (4)
Mn	2500	−2153 (1)	645 (1)	C(3)	783 (8)	−2975 (6)	−13 (4)
O(1)	2500	−4754 (9)	1849 (5)	C(4)	2500	−496 (12)	−62 (7)
O(2)	310 (6)	−3438 (5)	−426 (3)	B(1)	−1359 (12)	−497 (10)	1652 (6)
O(3)	−310 (6)	−3438 (5)	−426 (3)	B(2)	2500	−742 (16)	2589 (9)
O(4)	2500	511 (8)	−492 (6)	B(3)	1359 (12)	−457 (10)	1652 (6)
C(1)	2500	−3766 (11)	1396 (6)				

atom	x	y	z	B	atom	x	y	z	B
H(1)	−583	689	1400	4.0	H(5)	1238	−1269	2135	4.0
H(2)	2500	−2361	3033	4.0	H(6)	805	−1424	1304	4.0
H(3)	583	689	1400	4.0	H(7)	−805	−1424	1304	4.0
H(4)	−1269	−1269	2135	4.0					

[a] The standard deviations of the least significant digits are given in parentheses except for the arbitrarily fixed temperature factors of the hydrogen atoms and those fixed by symmetry in this table and all following tables.

Table III. Selected Interatomic Distances (Å) for $(CO)_4MnB_3H_7Br$[a]

Mn-C(C1)	1.867 (11)		
Mn-C(2)	1.821 (6)	Mn-C(3)	1.821 (6)
Mn-C(4)	1.859 (12)		
Mn-B(1)	2.356 (9)	Mn-B(3)	2.356 (9)
Mn-H(6)	1.777	Mn-H(7)	1.777
B(1)-B(2)	1.709 (15)	B(2)-B(3)	1.709 (15)
B(1)-B(3)	1.748 (18)		
B(1)-H(1)	1.260	B(3)-H(3)	1.260
B(1)-H(4)	1.053	B(3)-H(5)	1.053
B(1)-H(7)	1.113	B(3)-H(6)	1.113
B(2)-Br	2.033 (13)		
B(2)-H(2)	1.622		
B(2)-H(4)	1.286	B(2)-H(5)	1.286
C(1)-O(1)	1.138 (11)		
C(2)-O(2)	1.134 (7)	C(3)-O(3)	1.134 (7)
C(4)-(4)	1.130 (11)		

[a] Values tabulated on the right are symmetry related to those values appearing in the left column by the mirror plane located at $a/4$.

Table IV. Selected Intramolecular Bond Angles (Deg) for $(CO)_4MnB_3H_7Br$[a]

C(1)-Mn-C(2)	91.4 (3)	C(1)-Mn-C(3)	91.4 (8)
C(1)-Mn-C(4)	177.6 (4)		
C(1)-Mn-B(3)	96.0 (4)	C(1)-Mn-B(3)	96.0 (4)
C(1)-Mn-H(6)	86.4 (0)	C(1)-Mn-H(7)	86.4 (0)
C(2)-Mn-C(3)	92.5 (4)		
C(2)-Mn-C(4)	90.3 (3)	C(3)-Mn-C(4)	90.3 (3)
C(2)-Mn-B(1)	111.6 (3)	C(3)-Mn-B(3)	111.6 (3)
C(2)-Mn-B(3)	154.6 (3)	C(3)-Mn-B(1)	154.6 (3)
C(2)-Mn-H(6)	177.7 (0)	C(3)-Mn-H(7)	177.7 (0)
C(2)-Mn-H(7)	86.8 (0)	C(3)-Mn-H(6)	86.8 (0)
C(4)-Mn-B(3)	81.8 (4)	C(4)-Mn-B(1)	81.8 (4)
C(4)-Mn-H(6)	91.9 (0)	C(4)-Mn-H(7)	91.9 (0)
B(1)-Mn-B(3)	43.5 (4)		
B(1)-Mn-H(6)	69.5 (0)	B(3)-Mn-H(7)	69.5 (0)
B(1)-Mn-H(7)	26.9 (0)	B(3)-Mn-H(6)	26.9 (0)
H(6)-Mn-H(7)	93.8 (0)		
Mn-C(1)-O(1)	179.7 (9)		
Mn-C(2)-O(2)	177.6 (5)	Mn-C(3)-O(3)	177.6 (5)
Mn-C(4)-O(4)	179.9 (9)		
Mn-B(1)-B(2)	105.66	Mn-B(3)-B(2)	105.6 (6)
Mn-B(1)-B(3)	68.2 (2)	Mn-B(3)-B(1)	68.2 (2)
Mn-B(1)-H(4)	92.3 (0)	Mn-B(3)-H(5)	92.3 (0)
Mn-B(1)-H(7)	46.2 (0)	Mn-B(3)-H(6)	46.2 (0)
B(2)-B(1)-B(3)	59.2 (4)	B(2)-B(3)-B(1)	59.2 (4)
B(2)-B(1)-H(1)	128.9 (0)	B(2)-B(3)-H(3)	128.9 (0)
B(2)-B(1)-H(4)	48.7 (0)	B(2)-B(3)-H(5)	48.7 (0)
B(2)-B(1)-H(7)	118.8 (0)	B(2)-B(3)-H(3)	118.8 (0)
B(3)-B(1)-H(1)	118.1 (0)	B(1)-B(3)-H(3)	118.1 (0)
B(3)-B(1)-H(4)	95.1 (0)	B(1)-B(3)-H(5)	95.1 (0)
B(3)-B(1)-H(7)	112.4 (0)	B(1)-B(3)-H(6)	112.4 (0)
H(4)-B(1)-H(1)	139.1 (0)	H(5)-B(3)-H(3)	139.1 (0)
H(4)-B(1)-H(7)	75.8 (0)	H(5)-B(3)-H(6)	75.8 (0)
H(7)-B(1)-H(1)	109.9 (0)	H(6)-B(3)-H(3)	108.9 (0)
Br-B(2)-B(1)	112.9 (7)	Br-B(2)-B(3)	112.9 (7)
Br-B(2)-H(2)	117.9 (0)		
Br-B(2)-H(5)	128.7 (0)	Br-B(2)-H(4)	128.7 (0)
B(1)-B(2)-B(3)	61.5 (8)		
B(1)-B(2)-H(2)	119.7 (0)	B(3)-B(2)-H(2)	119.7 (0)
B(1)-B(2)-H(4)	38.0 (0)	B(3)-B(2)-H(5)	38.0 (0)
B(1)-B(2)-H(5)	88.9 (0)	B(3)-B(2)-H(4)	88.9 (0)
H(4)-B(2)-H(2)	83.8 (0)		
H(5)-B(2)-H(4)	97.5 (0)		
B(2)-H(4)-B(1)	93.3 (0)	B(2)-H(5)-B(3)	93.3 (0)
Mn-H(6)-B(3)	106.9 (0)	Mn-H(7)-B(1)	106.9 (0)

[a] Values tabulated on the right are symmetry related to those values appearing in the left column by the mirror plane located at $a/4$.

from a full variance–covariance matrix obtained from the final cycle of least-squares refinement.

Spectral Simulation

The complete line-shape analysis of experimental spectra was accomplished by visual comparison of actual data with spectra simulated by using the local program NMRSIM.[9] Input parameters include the chemical shift (Hz), as either the natural line width (Hz) at half-height or T_2 in seconds, the relative population of each exchanging site, and the rate constants for the one-step exchange between pairs of sites. Activation parameters and statistical analyses of experimental data were obtained by using the local program DEEJAY.[10]

Results and Discussion

The static molecular structure of $(CO)_4MnB_3H_7Br$ and the numbering system employed is illustrated in Figure 1, which shows the central manganese atom surrounded by an octahedral arrangement of four carbonyl groups and a bidentate B_3H_7Br ligand. The B_3H_7Br ligand is bound to the manganese through two Mn–H–B bridge hydrogen bonds. The bromine atom occupies an exo position on the unique boron, B(2), of the ligand. The B(1) and B(3) boron atoms are slightly below the plane formed by the two equatorial carbonyl groups and the manganese atom, while the B(2) boron atom lies slightly above the same plane. The plane formed by the triangular B_3 ring intersects the plane formed by B(1), B(3), and the manganese atom at an angle of 127°, which is somewhat greater than the corresponding angle observed in other bidentate B_3H_8 complexes.[11] The special symmetry location of the molecule on the crystallographic mirror plane at $a/4$ imparts ideal mirror plane symmetry to the molecular configuration. The unit cell configuration consists of discrete molecular entities, with the closest nonhydrogen contact distance of 3.164 Å found between O(3) and O(3) as related by the center of symmetry $(-x, -y, -z)$.

(9) Program NMRSIM was written by M.W.C. and D.F.H.; the work is based on: Reeves, L. W.; Shaw, K. N. *Can. J. Chem.* **1970**, *48*, 3641–53. A copy of this program is available from the authors on request.

(10) Weisman, G. R. Ph.D. Dissertation, University of Wisconsin–Madison, Madison, WI, 1976. This program was adapted to a Harris/7 computer.

(11) Hildebrandt, S. J.; Gaines, D. F.; Calabrese, J. D. *Inorg. Chem.* **1978**, *17*, 790–94 and references therein.

Table V. Anisotropic Thermal Parameters[a] ($\times 10^3$) for $(CO)_4MnB_3H_7Br$

atom	U_{11}	U_{22}	U_{33}	U_{12}	U_{13}	U_{23}
Br	52.7 (7)	86.9 (9)	61.7 (8)	0.0	0.0	−37.2 (7)
Mn	28.3 (7)	33.4 (7)	45.0 (8)	0.0	0.0	−5.6 (6)
O(1)	54 (4)	74 (5)	61 (5)	0.0	0.0	18 (4)
O(2)[b]						
O(3)	52 (3)	49 (3)	55 (3)	−7 (2)	−9 (2)	1 (2)
O(4)	56 (5)	46 (4)	106 (7)	0.0	0.0	23 (5)
C(1)	39 (5)	58 (7)	43 (5)	0.0	0.0	−3 (5)
C(2)[b]						
C(3)	33 (3)	30 (3)	44 (3)	−1 (3)	3 (3)	−3 (3)
C(4)	33 (5)	45 (5)	68 (7)	0.0	0.0	−6 (5)
B(1)[c]						
B(2)	46 (7)	79 (9)	60 (8)	0.0	0.0	−25 (7)
B(3)	39 (5)	75 (6)	90 (7)	1 (5)	−10 (5)	−28 (5)

[a] Anisotropic temperature factors are of the form $\exp[-2\pi^2 \times (U_{11}h^2a^{*2} + U_{22}k^2b^{*2} + U_{33}l^2c^{*2} + 2U_{12}hka^*b^* + 2U_{13}hla^*c^* + U_{23}klb^*c^*)]$. [b] Related by mirror plane symmetry to C(3) and O(3). [c] Related by mirror plane symmetry to B(3).

All distances and angles within the molecule are typical for bidentate $B_3H_8^-$ complexes.[11] The atomic coordinates and thermal parameters for all atoms are given in Table II. Selected interatomic distances and angles are presented in Tables III and IV, respectively. Anisotropic thermal parameters for the nonhydrogen atoms are given in Table V.

The final difference map revealed two unidentified peaks of 0.985 and 1.125 electrons. The positions of these peaks suggest the presence of a minor disorder in which some $(CO)_4MnB_3H_7Br$ molecules are located in inverted positions.

Internal Hydrogen Exchange in $(CO)_4MnB_3H_7Br$. A historical view of internal-exchange processes in boranes and related derivatives[12] indicates that, while there are many examples of internal hydrogen exchange that occur at rates that are amenable to study by NMR, there have been few successful attempts to study such exchange processes quantitatively. In addition, there are few examples of closely related borane derivatives that exhibit a broad range of internal hydrogen-exchange rates so that the effects of a small manageable number of compositional variables can be confidently assessed. The three complexes $(CO)_4MnB_3H_8$, $(CO)_4MnB_3H_7Br$, and $(CO)_3MnB_3H_8$ are closely related structurally but undergo internal hydrogen exchange at very different rates. The complex $(CO)_4MnB_3H_7Br$ was chosen for quantitative studies because of its high stability and convenient exchange rates which are readily observable under thermal conditions. The low-temperature ^1H NMR spectra of $(CO)_4MnB_3H_7Br$ at 270 MHz exhibit distinct resonances for each type of hydrogen present. When all ^{11}B resonances are adequately decoupled, line-shape analysis using the Reeves and Shaw formalism[9] is appropriate for the resultant spectra. At elevated temperatures the hydrogens H(2), H(1,3), and H(4,5) (Figure 1) undergo reversible internal exchange at increasing rates. This exchange process can be described by using a "jump" model[13] which involves the two-step process as shown in (1). During each "jump", a single pair of

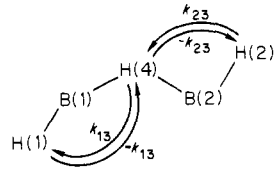

(1)

hydrogen atoms exchange positions at a rate, k_{ij}, which affects the shape of the observed NMR lines. The results of the total line-shape analysis of $(CO)_4MnB_3H_7Br$ are shown in Table VI. Temperature dependent rate constants are shown in Table VII. A comparison of experimental and calculated spectra is presented in Figure 2. The calculated activation parameters are within the expected range and exhibit error limits consistent with those

Table VI. Thermodynamic Activation Parameters and Eyring Plot[a] Constants for $(CO)_4MnB_3H_7Br$

parameter	k_{13}	k_{23}
$\Delta G^{\ddagger}$ (22 °C), kcal/mol	12.2 ± 0.3	12.2 ± 0.1
$\Delta H^{\ddagger}$, kcal/mol	9.6 ± 1.7	10.7 ± 0.7
$\Delta S^{\ddagger}$, eu	−8.8 ± 6.3	−5.1 ± 2.7
slope of $ln\ (k_{ij}/T)$ vs. $1/T$	−4833.1	−5405.0
intercept	18.64	20.52
correltn coeff	−0.964	−0.994

[a] To obtain $\Delta H^{\ddagger}$ and $\Delta S^{\ddagger}$ and to be able to compare $\Delta G^{\ddagger}$ values at different temperatures, we must make Eyring plots of $ln\ (k_{ij}/T)$ vs. $1/T$. The result is a straight line with slope $-\Delta H^{\ddagger}/R$ and intercept $ln\ (\kappa k_{jk}/h) + \Delta S^{\ddagger}/R$. $\Delta G^{\ddagger}$ values may then be calculated at any temperature from the definition $\Delta G^{\ddagger} = \Delta H^{\ddagger} - T\Delta S^{\ddagger}$.

Table VII. Rate Constants from the Total NMR Line Shape Analysis of $(CO)_4MnB_3H_7Br$ at Various Temperatures

temp, K	k_{13}, s^{-1}	k_{23}, s^{-1}
211	4.5	2
222	25	8
231	36	11
245	41	26
252	95	75
263	165	190
273	310	400
281	550	900
286	700	1200
296	1500	3000
304	11000	5500
310	14000	12000
320	25000	12000
328	25000	20000

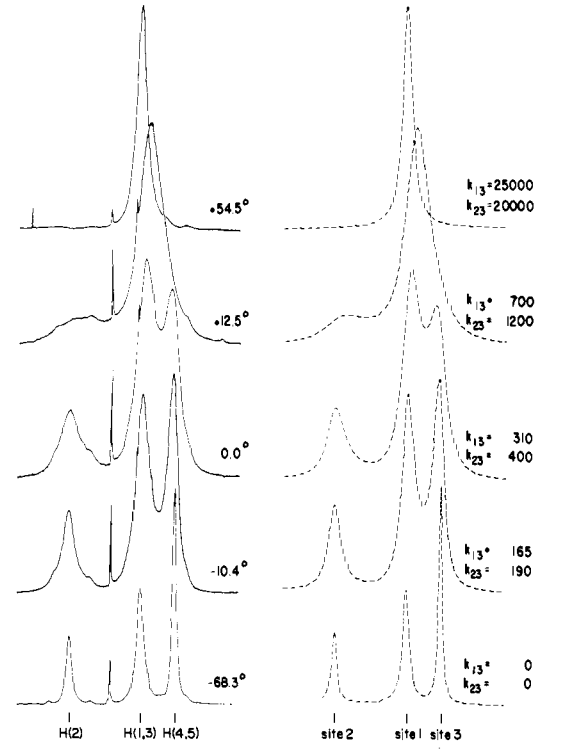

Figure 2. A comparison of selected experimental and theoretical spectra obtained in the total line-shape analysis of $(CO)_4MnB_3H_7Br$.

reported by other workers.[14] Calculations based on the "jump" model give information concerning the nuclear permutations which may occur during the exchange process but do not differentiate between various intramolecular pathways by which hydrogens may

(12) Beall, H.; Bushweller, C. H. *Chem. Rev.* **1973**, *73*, 465–86.
(13) Jesson, J. P; Meakin, P. *Acc. Chem. Res.* **1973**, *6*, 269–75.
(14) (a) Allerhand, A.; Chen, F.-M.; Gutowsky, H. S. *J. Chem. Phys.* **1965**, *42*, 3040–47. (b) Bushweller, C. H.; Gollni, J.; Rao, G. U; O'Neil, J. W. *J. Am. Chem. Soc.* **1970**, *92*, 3055–58.

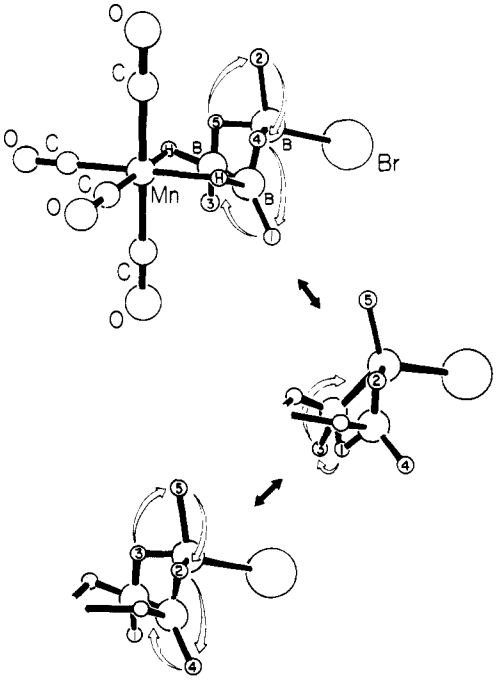

Figure 3. A proposed mechanism of intramolecular hydrogen exchange in $(CO)_4MnB_3H_7Br$.

exchange. Therefore, the final analytical step involves selection of suitable mechanistic exchange pathways based upon additional physical data and other knowledge of such systems.

The exo position of the bromine atom in $(CO)_4MnB_3H_7Br$ suggests the following proposal for the mechanism of intramolecular exchange of the boron-bound hydrogens (hydrogens involved in the M-H-B bridge bonding are not involved in the exchange process). The NMR spectra show that each boron atom possesses one coordination site which is not involved in the hydrogen exchange. The *styx* "2013" formulation, seen in eq 2, A and C, show the H(6), H(7), Br positions, which remain static,

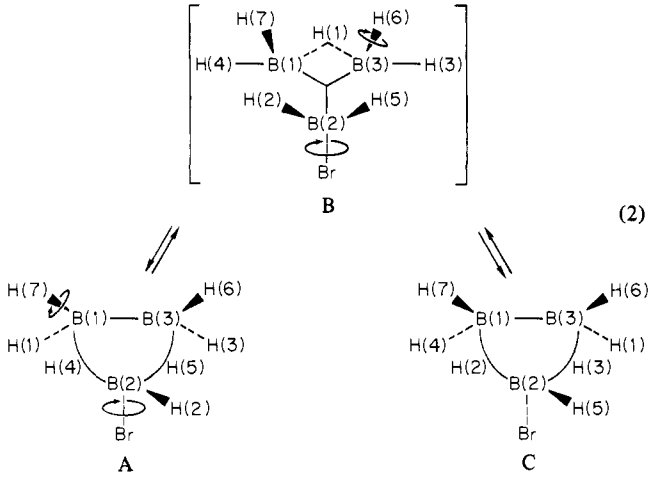

and the dynamic hydrogen atoms which occupy the exchange-allowed sites. The transition state, a *styx* "1104" formulation, contains a three-center BBB bond and a single BHB bridge bond, as shown in eq 2, B. The hydrogen-exchange process can be initiated by rotation around the B-Br bond coupled with rotation about either B-H bond in the metal-boron bridge. These coupled rotations form the "1104" intermediate shown in eq 2, B, which may also be represented by a "2013" designation as is shown in the perspective sketches in Figure 3. Continued rotation about the B-Br bond and the opposite metal bridge B-H bond in the "1104" species carries bridge hydrogens to terminal positions in a "new" "2013" species as seen in eq 2, C. Exhaustive repetition of this two-step mechanism leads to total equivalence of B-H-B

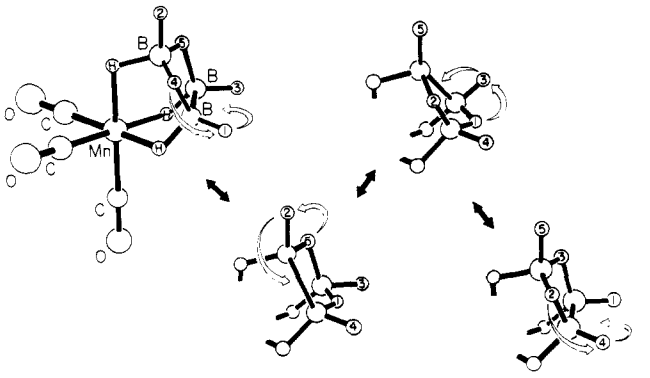

Figure 4. A proposed mechanism of intramolecular hydrogen exchange in $(CO)_3MnB_3H_8$.

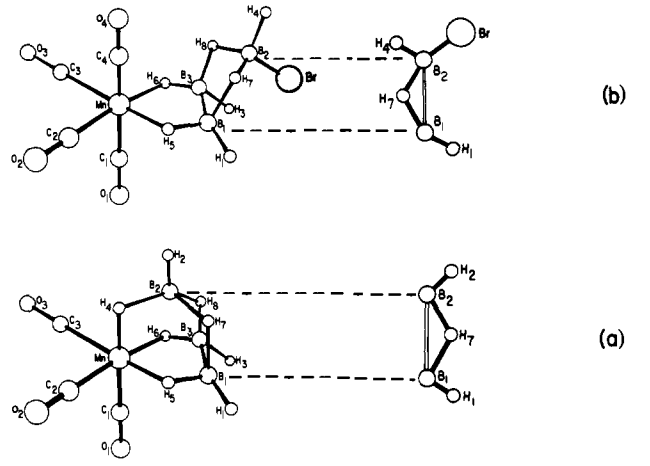

Figure 5. A comparison of the proposed mechanistic exchange processes in $(CO)_4MnB_3H_7Br$ and $(CO)_3MnB_3H_8$.

bridge and B-H terminal hydrogen atoms with minimal atom motion.

A closely related exchange process is undoubtedly occurring in the related complex $(CO)_3MnB_3H_8$.[15] NMR studies indicate that the site transfer of the five boron-bound hydrogen atoms in $(CO)_3MnB_3H_8$ is sufficiently rapid on the NMR time scale that a static configuration cannot be observed at temperatures as low as -80 °C.[1] As in $(CO)_4MnB_3H_7Br$, the hydrogen atoms involved in M-H-B bridge bonding in $(CO)_3MnB_3H_8$ are not participants in the intramolecular exchange process. On the basis of the much lower barrier to exchange in $(CO)_3MnB_3H_8$ and its tridentate ligand-metal bonding, we propose that the most reasonable exchange mechanism consists of a cascade effect in which coupled rotations about metal-boron bridge bonds serve to carry bridge and terminal hydrogen atoms around the B_3 ring, as shown in Figure 4. A comparison of the idealized molecular structures and a simplified representation of their differences in the proposed site-exchange pathways for $(CO)_3MnB_3H_8$ and $(CO)_4MnB_3H_7Br$ is shown in Figure 5. The stereochemistry of $(CO)_3MnB_3H_8$ places all the boron-bound hydrogens on one side of the B_3 triangle, as shown in Figure 5a. Intramolecular exchange, therefore, occurs exclusively over the face of the B_3 ring. Such an exchange should presumably be very facile, commensurate with the experimental data. The requirement of a fixed bromine atom in $(CO)_4MnB_3H_7Br$ adds a different constraint to its site exchange system. As shown in Figure 5b, the hydrogens involved in this exchange process must pass from one side of the B_3 ring to the opposite side. This somewhat more radical alteration of the hydrogen position can reasonably be expected to give rise to a higher activation barrier, as is observed.

While both $(CO)_4MnB_3H_7Br$ and $(CO)_3MnB_3H_8$ are stereochemically nonrigid species at ambient temperature, the parent

(15) Hildebrandt, S. J.; Gaines, D. F.; Calabrese, J. C. *Inorg. Chem.* **1978**, *17*, 790-94.

compound, $(CO)_4MnB_3H_8$, remains static under ordinary conditions. However, $(CO)_4MnB_3H_8$ also exhibits internal hydrogen exchange, as observed by ^1H NMR spectra at temperatures >80 °C. Elevated temperatures appear to promote the exchange of hydrogen atoms between B-H-B bridge and B-H terminal positions. However, within the BH_2 group, it is clear that one of the terminal hydrogen atoms is not involved in the exchange process. If the endo, H(4), position is excluded from the exchange process, a mechanism similar to that proposed for $(CO)_3MnB_3H_8$ may occur. If the exo-hydrogen atom is excluded from the exchange process, a mechanism identical with that proposed for $(CO)_4MnB_3H_7Br$ may obtain.

At present, there are no methods for stereospecific labeling of the BH_2 unit of $(CO)_4MnB_3H_8$. In addition, extensive decomposition of $(CO)_4MnB_3H_8$ occurs at the elevated temperatures required to effect rapid exchange. If it is assumed, however, that the exchange behavior is mechanistically similar to the process observed in $(CO)_4MnB_3H_7Br$, a reconstruction of the Eyring plots adjusted to a new temperature range (+30 → +150 °C), using predetermined rate constants and assuming spectral coalescence at ~100 °C, yields an estimated $\Delta G^{\ddagger}$(100 °C) of approximately 16 kcal/mol for $(CO)_4MnB_3H_8$. When similar assumptions are applied to the $(CO)_3MnB_3H_8$ system (static structure at -200 °C, coalescence temperature -165 °C, a $\Delta G^{\ddagger}$(-165 °C) of approximately 5 kcal/mol is obtained. This latter value is similar to the upper limit estimated for the potential barrier to pseudorotation in TlB_3H_8 and $(CH_3)_4NB_3H_8$[16] and is somewhat greater than the barrier to hydrogen exchange calculated for the free gas-phase $B_3H_8^-$ anion.[17]

Acknowledgments. This work was supported in part by grants, including departmental instrument grants for NMR and X-ray facilities, from the National Science Foundation.

(16) Bushweller, C. H.; Beall, H.; Grace, M.; Dewkett, W. J.; Bilofsky, H. S. *J. Am. Chem. Soc.* **1971**, *93*, 2145-49.
(17) Pepperberg, I. M.; Dixon, D. A.; Lipscomb, W. N.; Halgren, T. A. *Inorg. Chem.* **1978**, *17*, 587-93.

Mechanisms of 1,1-Reductive Elimination from Palladium

Arlene Gillie and J. K. Stille*

Contribution from the Department of Chemistry, Colorado State University, Fort Collins, Colorado 80523. *Received February 8, 1980*

Abstract: The 1,1-reductive elimination of ethane from three *cis*-bis(phosphine)dimethylpalladium complexes, $L_2Pd(CH_3)_2$ (L = PPh_3,PPh_2CH_3; L_2 = $Ph_2PCH_2CH_2PPh_2$), and three trans analogues [L = PPh_3, PPh_2CH_3; L_2 = 2,11-bis(diphenylphosphinomethyl)benzo[*c*]phenanthrene (TRANSPHOS)] was carried out. The three cis complexes underwent reductive elimination in the presence of coordinating solvents (Me_2SO, DMF, THF). The trans complexes which could isomerize to cis (L = PPh_3, PPh_2CH_3) did so in polar solvents and then underwent reductive elimination. (TRANSPHOS)dimethylpalladium would not undergo reductive elimination of ethane, even at 100 °C in Me_2SO. The eliminations from the cis isomers were intramolecular as determined by the lack of crossover with the perdeuteriomethylpalladium analogue and displayed first-order kinetics (k = 1.04×10^{-3} s^{-1}, L = PPh_3, 60 °C; K = $(6.5\text{-}9.5) \times 10^{-5}$ s^{-1}, L = PPh_2CH_3, 60 °C; k = 4.78×10^{-7} s^{-1}, L_2 = $Ph_2PCH_2CH_2PPh_2$, 80 °C). The presence of diphenylacetylene in the reaction mixture traps the palladium(0) product as the bis(diphenylmethylphosphine)(diphenylacetylene)palladium complex. Although (TRANSPHOS)dimethylpalladium would not undergo a 1,1-reductive elimination of ethane, the addition of CD_3I to a Me_2SO solution of this complex at 25 °C rapidly produced CD_3-CH_3, implicating a transient palladium(IV) intermediate.

Introduction

The coupling reaction of organic compounds catalyzed by transition metals is an important method of generating carbon-carbon bonds, the final step of which requires the elimination of the organic partners from the transition metal. The reductive elimination can take one or more paths, categorized according to the mechanism (and products), including heterolytic as well as homolytic or concerted α elimination, β elimination, 1,1-reductive elimination, and dinuclear elimination.[1-6] In the 1,1-reductive elimination reaction, the formal oxidation state and the coordination number of the metal are reduced by two; bond breaking is accompanied by bond making. The reductive elimination reaction frequently follows an oxidative addition reaction, and this combination, oxidative addition-reductive elimination, is responsible for both stoichiometric and catalytic coupling reactions via transition metals, particularly those of group 8. Critical mechanistic studies on the 1,1-reductive elimination reactions of diorganopalladium complexes are scarce, yet palladium has been demonstrated to catalyze a large number of different coupling reactions in which reductive elimination is part of the sequence.

Palladium(0) catalyzes the coupling of benzyl halides with organometals, such as Grignard reagents and organolithium compounds. In a number of studies the 1,1-reductive elimination of organic partners from bis(phosphine)diorganopalladium(II) complexes has been carried out as a model for that step in the catalytic coupling reaction[7,8] (eq 1c). For example, *trans*-bis(phosphine)methylphenylpalladium(II) complexes decompose thermally to give toluene.[7] One of the problems to be examined in such a 1,1-reductive elimination reaction, therefore, is the mechanism by which the two trans organic partners eventually become coupled. In catalytic coupling reactions proceeding by the oxidative addition-methathesis sequence, the trans complex

(1) Norton, J. R. *Acc. Chem. Res.* **1979**, *12*, 139.
(2) Davidson, P. J.; Lappert, M. F.; Pearce, R. *Chem. Rev.* **1976**, *76*, 219; *Acc. Chem. Res.* **1974**, *7*, 209.
(3) Parshall, G. W. *Acc. Chem. Res.* **1975**, *8*, 113.
(4) Kochi, J. K. *Acc. Chem. Res.* **1974**, *7*, 351.
(5) Baird, M. C. *J. Organomet. Chem.* **1974**, *64*, 289.
(6) Braterman, P. S.; Cross, R. J. *Chem. Soc. Rev.* **1973**, *2*, 271.
(7) Parshall, G. W. *J. Am. Chem. Soc.* **1974**, *96*, 2360.
(8) Ito, T; Tsuchiya, H.; Yamamoto, A. *Bull. Chem. Soc. Jpn.* **1977**, *50*, 1319.

0002-7863/80/1502-4933$01.00/0